ChemComm

Accepted Manuscript

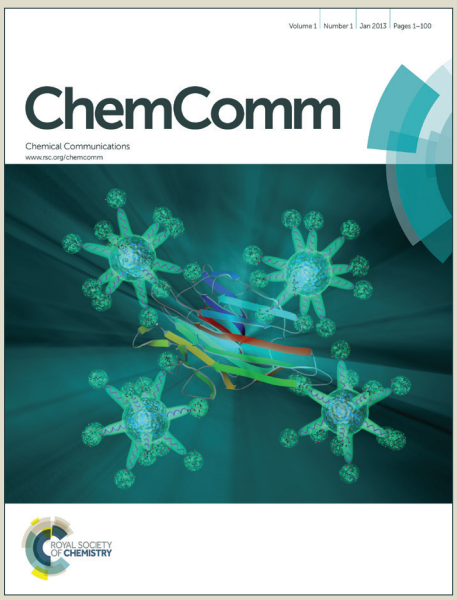

ROYAL SOCIETY OF CHEMISTRY

www.rsc.org/chemcomm

Cite this: DOI: 10.1039/c0xx00000x

www.rsc.org/xxx

ARTICLE TYPE

Unstable-Fe-sites induced formation of mesopores in microporous zeolite Y without organic template

Dongdong Guo,[a] Baojian Shen,*[a] Guodong Qi,[b] Liang Zhao,[a] Jun Xu,[b] Feng Deng,[b] Yuchen Qin,[a] Qiaoxia Guo,[a] Shenyong Ren,[a] Xionghou Gao,[c] Song Qin,[d] Baojie Wang,[c] Hongjuan Zhao,[c] Honghai Liu,[c] Xinmei Pang[c]

Received (in XXX, XXX) XthXXXXXXXXX 20XX, Accepted Xth XXXXXXXXX 20XX
DOI: 10.1039/b000000x

A novel organic-free strategy for generating mesoporosity in Y zeolite is reported. It is revealed that Fe^{3+} functioned as unstable sites in Fe-NaY zeolite, which promotes deferrization-dealumination, leading to enhanced formation of intra-crystalline mesoporosity as well as desirable interconnectivity. The mesopores-enriched zeolite exhibits a remarkable ability in bulky substrate conversion.

Zeolites typically have high activities in heterogeneous catalysis processes, but their micropores with aperture diameter below 1 nm greatly limit their utilization in reactions involving large molecules or macromolecules[1]. A great deal of efforts have been devoted to overcoming this pore-size limitation of zeolites by reducing the diffusion path lengths, such as nano-crystal-size of zeolites[2], exfoliating layered zeolites[3], zeolite-seed-assembled mesoporous materials with amorphous framework[4], introducing mesopores in the microporous material by templating strategies[5] or dealumination[6]. Recently, desilication by base leaching has attracted intensive attention due to the capability to form of mesopores[7,8]. However, this desilication can not be exploited to generate mesopores in ordinary zeolite NaY because of its low SiO_2/Al_2O_3 ratio[9,10]. Our previous work indicated that mesoporous ultra-stable Y (USY) zeolite could be prepared through the sequential desilication–dealumination process by using a high silica NaY zeolite as the starting material, in which the desilication afforded textural defects affecting the initiation of mesopores in crystal parts and promoting the following propagation and coalescence of mesopore[11,12]. Nevertheless, it is still a challenge to directly construct abundant and well interconnected mesopores in microporous zeolite without desilication or organic template-free strategy. On the other hand, the known successful steaming dealumination temperature is usually performed at above 600 °C, if a steaming treatment process at lower temperature can be developed, it will be very attractive. Therefore, it is interesting for us to try to realize a similar ultra-stabilization at the temperature as low as possible, however, to our knowledge, no report about lower steaming temperature treatment has been published so far. Thus, it is reasonable for us to propose that, to excavate intra-crystalline mesopores, some part of microporous zeolite structure should be corrupted easily. This may be achieved by the introduction of unstable sites which can be moved away upon post-treatment.

Herein, we report a novel strategy to generate mesopores by incorporating Fe atoms into framework of NaY during hydrothermal synthesis process, and then deferrization-dealumination via steaming.

Iron-containing FAU type Fe-NaY and NaY zeolites were synthesized by hydrothermal method without using organic template (see Fig. S1 for XRD patterns). Direct evidence of the incorporation of Fe in the zeolite framework sites was observed by performing unit cell parameter (Table S1), combination of UV-Vis-DRS and UV Raman (Fig. S2), and ESR (Fig. S3). This material has a typical microporous feature (*t-plot*, Table S1), accordingly, no contribution of mesopores was presented in the pore size distribution obtained from the adsorption branch (data not shown), which was in line with TEM studies where no contrast was distinguished throughout the crystals of the Y zeolites. However, the result of ^{27}Al MAS NMR showed that the half band width of the framework Al line of Fe-NaY was broader than that of NaY sample (Fig. S4), which indicated significant distortions in framework Al leading to an increase in quadrupole interaction, meanwhile, partial framework Fe existed in Y zeolite with distorted tetrahedral coordinations according to ESR analysis (Fig. S3). This suggested a weakened zeolite structural unit induced by the Fe substitution. The fact that the lattice collapse temperature of the Fe-NaY zeolite was 79 °C lower than that of the NaY zeolite supports our hypothesis (Fig. S5 for the details of the TG/DSC curves). The above analysis was substantiated by DFT calculations (Supporting Information). We propose that the existence of "unstable Fe^{3+} sites" distorted of framework Al, which decreased the structural stability.

The Na^+ cations were ion exchanged by ammonium ions and the resulting zeolites were followed by steam treatment to obtain samples USY (from NaY) and USY_{Fe} (from Fe-NaY). Details about the samples were summarized in Table 1. The result indicated that Fe content of USY_{Fe} sample is 0.13 wt. %. Meanwhile, the combination of deferrization and dealumination improved the efficiency of dealumination around the Fe center and thus increased the framework SiO_2/Al_2O_3 molar ratio of USY_{Fe}. When the samples were steamed at 650 °C for 2 h, the SiO_2/Al_2O_3 was increased by 3.8 for USY_{Fe} (18.4) compared with USY (14.6). It was very surprising to note that the molar ratio of framework SiO_2/Al_2O_3 could still be achieved at 13.6 when the

Table 1. The chemical composition and porosity data of the USY and USY_{Fe} zeolites

Sample	Fe content[a] [wt. %]	SiO_2/Al_2O_3[b]	a_0 [nm]	S_{BET} [m^2g^{-1}]	S_{exter} [m^2g^{-1}]	V_{pore} [cm^3g^{-1}]	V_{micro} [cm^3g^{-1}]	V_{meso}[c] [cm^3g^{-1}]
USY	0.04	14.6	2.439	613	73	0.42	0.27	0.15
USY_{Fe}	0.13	18.4	2.435	592	84	0.46	0.25	0.21

[a]XRF. [b]Framework SiO_2/Al_2O_3 molar obtained from XRD analysis data by using Breck-Flanigen equation. [c]$V_{meso} = V_{pore} - V_{micro}$.

steamimg treatment temperature decreased by 100°C (550 °C, 2 h) for Fe-NaY. It was analogous to the value of 14.6 for the above mentioned USY, which was obtained at 650 °C for 2 h steaming. The result indicated that the steaming treatment could be performed at lower temperature compared to the usual case of 650 °C. This finding will not only reduce energy consumption, but also decrease the operation severity and thus be beneficial to equipment requirement. Some papers and reviews[6,13] which described the preparation of dealuminated zeolites have emphasized that the skeleton stability, the hydrothermal stability, the thermal stability and acidity intensity could be improved to a great extent by increasing the SiO_2/Al_2O_3 ratio of a low silica zeolite. It was important to notice that the structural stability of the USY_{Fe} increased by 20 °C compared with USY (see Fig. S6 for TG/DSC patterns). In addition, the results of acid sites obtained by Py-IR as shown in Table S2 and indicated that the total number of acid sites was somewhat lower for the USY_{Fe}, however, the medium and strong acid sites of USY_{Fe} were a little bit more than that of USY, and in agreement with the NH_3-TPD measurement (Fig. S7). These observations are well consistent with their SiO_2/Al_2O_3 ratios between USY_{Fe} and USY.

The porosity of the samples was studied by nitrogen physisorption. Fig. 1 displayed the adsorption–desorption isotherms as well as the pore size distributions derived from the desorption branches. The data related to these measurements were collected in Table 1. The nitrogen isotherm of USY and USY_{Fe} exhibited a step at a relative pressure of 0.45~1.0, which is typically assigned to the presence of mesopore. Mesostructured zeolites that contained mesopores centered at around 9 nm for USY and 17 nm for USY_{Fe} were obtained. The data in Table 1 revealed that the mesopore volume of USY_{Fe} zeolite was increased by 40 % compared to USY zeolite. Clearly, the steaming of Fe-NaY is particularly effective in generating the mesopore network in this material.

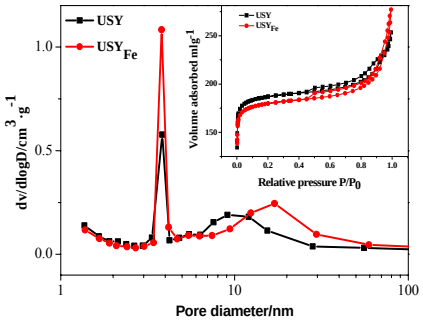

Fig. 1 BJH pore size distribution derived from the desorption branches of isotherms and N_2 adsorption-desorption isotherms for the USY and USY_{Fe} zeolites.

To get a better understanding about the porosity of porous materials, ^{129}Xe NMR of adsorbed xenon was used to probe them[14]. Fig. 2 showed the ^{129}Xe NMR spectra of xenon adsorbed in USY and USY_{Fe} with adsorption pressure of xenon varying from 9.0×10^2 to 5.4×10^4 Pa. For USY (Fig. 2a), only one signal was presented in the ^{129}Xe NMR spectrum due to a fast exchange of xenon atoms adsorbed in the micropores with those in the mesopores during the NMR time scale. The observation of one ^{129}Xe signal over a wide range of xenon pressures implied that there is only one type of hierarchical pores in the USY crystal and the connection between the mesopores was through the intrinsic micropores[15]. For the USY_{Fe} (Fig. 2b), at low xenon pressure, two signals at about 67 and 63 ppm were observed. In analogy to the signal in USY, the former signal (67 ppm) could be assigned to the xenon atoms adsorbed in both micropores and mesopores with fast exchange, while the latter one (63 ppm) could be attributed to the xenon atoms adsorbed in another type of mesopores which were also undergoing fast exchange with those adsorbed in either micropores or mesopores. Increasing adsorption pressure of xenon led to coalescent of the two signals, which indicated fast exchange of Xe among the various micropores/mesopores. This suggests that there is a good communication among various types of pores in USY_{Fe} sample.

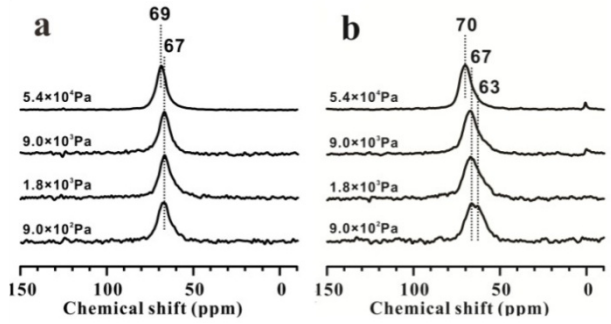

Fig. 2 Pressure-dependent ^{129}Xe NMR spectra (acquired at room temperature) of xenon adsorbed in USY (a) and USY_{Fe} (b) zeolites.

Evidence of the homogeneous distribution of mesopores through the crystals of USY and USY_{Fe} zeolites was demonstrated by TEM observation of thin sections of ultramicrotomed slices of the crystals as shown in Fig. 3, and 3D reconstructions of zeolite crystals were obtained and analyzed (Fig. S8). For USY_{Fe}, dense light spherical mesopores were pervasive throughout the thin slice (Fig. 3b) mainly observed as pearl necklace-like chain involving an end-to-end overlap, which were in line with 3D-TEM (Fig. S8d), whereas for the USY zeolite (Fig. 3a and Fig. S8c), it was shown that the mesopores were very inhomogeneously distributed in single zeolite particles and in different crystals.

With respect to the mechanism of the generation of the mesopores, it is indicated that the introduction of "unstable Fe^{3+} sites" enhances the distortion of framework aluminum of pristine Y zeolite, which makes the zeolite unstable and more sensitive to further treatment. On the other hand, the "unstable Fe^{3+} sites" are easily dislocated from the framework during steaming (since the bond energy of Fe-O is lower than that of Al-O) to generate struc-

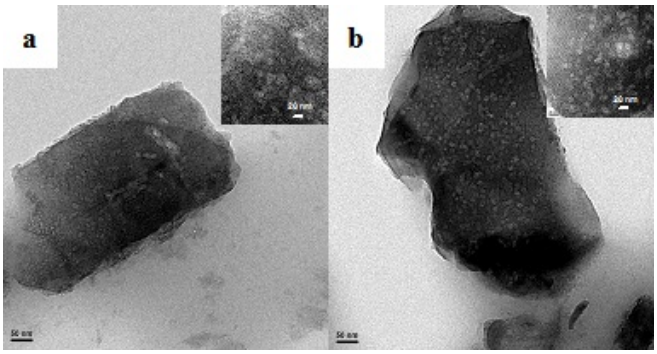

Fig. 3 TEM images of the thin slices of USY(a) and USY_{Fe}(b) zeolites.

-tural defect sites according to ESR analysis (Fig. S9), which provides channels for diffusion of water molecules to promote the hydrolysis of the surrounding Si-O-Al bonds, and thus facilitates the formation of uniform mesopores throughout the zeolite crystals. As anticipated based on differences in mesoporosity, the bulkier TIPB (1,3,5-triisopropylbenzene) catalytic cracking results in Fig. 4 illustrated the superior reactivity of USY_{Fe}. Although both of them gradually lost activity with time on stream, the USY_{Fe} zeolite showed a much slower deactivation rate than the USY zeolite. Fig. S10 showed the Arrhenius plots of the monomolecular cracking of TIPB. The apparent activation energies of cracking over USY and USY_{Fe} were 57 and 46 $kJ \cdot mol^{-1}$, respectively. This suggested that the apparent activation energies was decreased by 11 $kJ \cdot mol^{-1}$ over USY_{Fe} zeolite. It was clear that the improved catalytic performance in conversion of bulky substrate TIPB and the decreased apparent activation energy on the USY_{Fe} zeolite were closely related to its upgraded mesoporosity system. For further investigation of the improvement in the mesoporosity, heavy oil was used as feedstock to prove useful for applications as shown in Table S3. Our studies indicated that the USY_{Fe} catalyst showed a significant increase towards the yield of gasoline and LCO compared to the USY catalyst, meanwhile, the undesired products such as dry gas, LPG, coke, and bottoms decreased. It is evident from our studies[12] that the higher gasoline and lower coke yield by using the mesopores-enriched catalyst was attributed to rapid mass transfer of intermediate products from the mesopores, thus secondary cracking (such as to LPG) was almost fully suppressed. This conclusion is qualitatively in line with the recently introduced hierarchy factor[16].

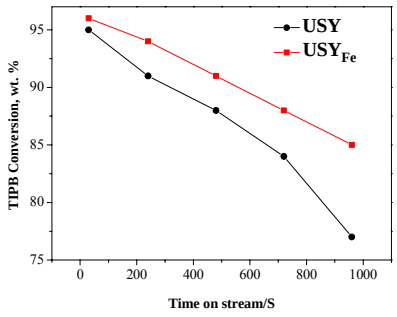

Fig. 4 TIPB conversion versus time on stream for the USY and USY_{Fe} zeolites.

In summary, unstable Fe^{3+} sites are introduced in the NaY framework and it is used as a strategy to generate mesoporous structures for improving molecule diffusion. It is revealed that the Fe^{3+} ions functioned as the unstable sites, which could promote the deferrization-dealumination leading to a high efficiency of dealumination around Fe centers. As a result, the mesopore volume and thermal stability of the zeolite are increased by over 40 % and 20 °C, respectively, compared with the USY. Furthermore, it could be observed that a similar ultra-stabilization can be achieved at lower steaming temperature. Consequently, the mesoporous-enriched zeolite exhibits the enhanced activity. In addition, it can improve the yield of gasoline from the cracking of heavy oil. We anticipate that the concept of "unstable-site" developed in the present work will be applied to the preparation of other hierarchically structured materials.

Notes and references

[a]*State Key Laboratory of Heavy Oil Processing, China University of Petroleum, Beijing 102249, China. Fax: 86 10 89733369; Tel: 8610 89733369; E-mail: baojian@cup.edu.cn.*
[b]*Wuhan Center for Magnetic Resonance, Wuhan Institute of Physics and Mathematics, The Chinese Academy of Sciences, Wuhan, China.*
[c]*Lanzhou Petrochemical Research Center, Petrochemical Research Institute, PetroChina Company Limited, Lanzhou, China.*
[d]*Catalyst Plant of Lanzhou Petrochemical Company, PetroChina Company Limited, Lanzhou, China.*

†Electronic Supplementary Information (ESI) available: Characterization, preparation details and supporting spectra. See DOI: 10.1039/b000000x/

‡We acknowledge the funding of this project by MOST ''973'' Project of China (2012CB215001) and Key Technologies R&D Program of China (2012BAE05B02).

1 A. Corma, J. Catal., 2003, 216, 298; Y. Tao, H. Kanoh, L. Abrams and K. Kaneko, Chem. Rev., 2006, 106, 896; K. Egeblad, C. H. Christensen and M. Kustova, *Chem. Mater.*, 2008, **20**, 946.
2 L. Tosheva and V. P. Valtchev, *Chem. Mater.*, 2005, **17**, 2494.
3 A. Corma, V. Fornes, S. B. Pergher, Th. L. M Maesen and J. G. Buglass, *Nature*, 1998, 396, 353; A. Corma, U. Diaz, M. E. Domine and V. Fornés, *J. Am. Chem. Soc.*, 2000, **122**, 2804.
4 F. Sh. Xiao, Y. Han, Y. Yu, X. J. Meng, M. Yang and Sh. Wu, *J. Am. Chem. Soc.*, 2002, **124**, 888.
5 F. Sh. Xiao, L. F. Wang, C. Y. Yin, K. F. Lin, Y. Di, J. Li, R. Xu, D. S. Su, R. Schlogl, T. Yokoi and T. Tatsumi, *Angew. Chem., Int. Ed.*, 2006, **45**, 3090.
6 R. A. Beyerlein, C. Choi-Feng, J. B. Hall, B. J. Huggins and G. J. Ray, Top. Catal., 1997, 4, 27; H. K. Beyer, *Springer*, 2002, **3**, 203.
7 J. C. Groen, W. Zhu, S. Brouwer, S. J. Huynink, F. Kapteijn, J. A. Moulijn and J. Pérez-Ramírez, *J. Am. Chem. Soc.*, 2007, **129**, 355; J. C. Groen, S. Abelló, L. A. Villaescusa and J. Pérez-Ramírez, *Microporous Mesoporous Mater.*, 2008, **114**, 93.
8 A. Bonilla, D. Baudouin and J. Pérez-Ramírez, *J. Catal.*, 2009, **265**, 170.
9 J. C. Groen, J. C. Jansen, J. A. Moulijn and J. Pérez-Ramírez, *J. Phys. Chem. B*, 2004, **108**, 13062.
10 D. Verboekend, G. Vilé and J. Pérez-Ramírez, *Adv. Funct. Mater.*, 2012, **22**, 916.
11 Zh. X. Qin, B. J. Shen, X. H. Gao, F. Lin, B. J. Wang and Ch. M. Xu, *J. Catal.*, 2011, **278**, 266.
12 Zh. X. Qin, B. J. Shen, Zh. W. Yu, F. Deng, L. Zhao, Sh. G. Zhou, D. L.Yuan, X. H. Gao, B. J. Wang, H. J. Zhao and H. H. Liu, *J. Catal.*, 2013, **298**, 102.
13 J. Scherzer, *Appl. Catal.*, 1991, **75**, 1.
14 J. Demarquay and J. Fraissard, *Chem. Phys. Lett.*, 1987, **136**, 314; J. L. Bonardet, J. Fraissard, A. Gédéon and M. A. Springuel-Huet, *Catal. Rev. Sci. Eng.*, 1999, **41**, 115.
15 P. Kortunov, S. Vasenkov, J. Kärger, R. Valiullin, P. Gottschalk, M. Fé Elía, M. Perez, M. Stöcker, B. Drescher, G. McElhiney, C. Berger, R. Gläser and J. Weitkamp, *J. Am. Chem. Soc.*, 2005, **127**, 13055.
16 J. Pérez-Ramírez, S. Abelló, A. Bonilla and J. C. Groen, *Adv. Funct. Mater.*, 2009, **19**, 164.